JOURNAL OF SOLID STATE CHEMISTRY 70, 281–294 (1987)

Vacancy Induced Changes in the Electronic Structure of Titanium Nitride*

P. HERZIG,† J. REDINGER,‡ R. EIBLER,† AND A. NECKEL†

†*Institut für Physikalische Chemie, Universität Wien, Währingerstrasse 42, A-1090 Vienna, Austria, and* ‡*Institut für Technische Elektrochemie, Technische Universität Wien, Getreidemarkt 9, A-1060 Vienna, Austria*

Received December 28, 1986

A self-consistent APW band structure calculation has been performed for $TiN_{0.75}$, assuming long-range ordered vacancies at the nonmetal lattice sites. Two different kinds of titanium atoms occur in this model: $Ti^{[6]}$ atoms that are octahedrally surrounded by six nitrogen atoms and $Ti^{[4]}$ atoms that have only four nitrogen neighbors and are adjacent to two vacancies. The model structure can be described as $Ti_3^{[4]}Ti^{[6]}N_3\square_N$, where $\square_N$ denotes a nitrogen vacancy. In the densities of states, two sharp vacancy peaks have been found which are not present in stoichiometric TiN. The bonding situation is discussed by means of electron density plots. It is found that the chemical bonding is characteristically influenced by the introduction of vacancies. The calculated XPS and K XES are shown to be in good agreement with the experimental spectra.

Introduction

In two recent papers (*1*, *2*) the influence of vacancies at the carbon sublattice sites on the electronic structure of titanium carbide was studied by means of a self-consistent APW band structure calculation for the hypothetical ordered compound $TiC_{0.75}$. An analysis of the electron densities resulting from the band structure calculations clearly indicated that by replacing carbon atoms by vacancies, which entails a reduction of the number of Ti–C bonds, new bonds are formed between the Ti atoms surrounding the vacancy. The strengthening of the metal–metal bonds has already been predicted as early as 1953 by Nowotny (*3*).

In the light of our investigations on $TiC_{0.75}$ it seems promising to perform a comparative analysis of the influence of vacancies on the bonding properties of the related compounds $TiN_{0.75}$ and $TiO_{0.75}$ (*4*). Moreover, such a comparison might furnish an explanation for the fact that vacancies occur exclusively on the nonmetal lattice sites for the carbide and, apart from preparations under special experimental conditions, also for the nitride (*5*), whereas stoichiometric TiO contains 15% vacancies on both the Ti and O sublattices (*6*) under normal experimental conditions. The present work deals with the electronic structure of nitrogen-deficient titanium nitride.

TiN_x crystallizes in the sodium chloride structure in the composition range $0.61 \leq x \leq 1.00$ (*7*), with vacancies only on the N sublattice for thermodynamically stable

* Dedicated to Dr. H. Nowotny.

0022-4596/87 $3.00

samples. For $x = 0.61$, a long-range ordered vacancy structure was found to exist (*5*). A certain amount of short-range order can be detected for samples with low nitrogen contents ($x \lesssim 0.75$) (*8*). For $x \gtrsim 0.75$ the vacancies on the nitrogen sublattice appear to be disordered (*8*).

Recently KKR-CPA calculations have been published for the densities of states (DOS) in substoichiometric titanium nitrides of varying vacancy contents (*9, 10*). In those calculations the vacancies are assumed to be statistically distributed over the nonmetal sites without allowing for either short-range or long-range order. Apart from the expected reduction of the partial nitrogen *s* and *p* DOS the authors obtain two additional "vacancy" peaks near the Fermi level which can also be seen in recently measured XPS spectra (*11, 12*) but which were not found in an earlier tight-binding CPA calculation (*13*). However, CPA calculations cannot, in principle, supply information on particular bonds in a crystal. In order to study chemical bonding we performed a conventional APW supercell band structure calculation for vacancy-ordered $TiN_{0.75}$, adopting the same superstructure as for $TiC_{0.75}$ (*1, 2*). Although $TiN_{0.75}$ does not appear to be long-range ordered, the conclusions concerning the influence of vacancies on the chemical bonding should nevertheless be valid.

Computational Aspects

A self-consistent APW band structure calculation (*14*) has been performed for stoichiometric TiN and for the hypothetical ordered $TiN_{0.75}$ ($Ti_3^{[4]}Ti^{[6]}N_3\square_N$; see Fig. 1 for the model structure). The vacancy $\square_N$ in the center of the cubic unit cell is octahedrally surrounded by six $Ti^{[4]}$ atoms which have only four nearest N neighbors. The $Ti^{[6]}$ atoms at the corners of the cell are surrounded by six N neighbors as in stoichiometric TiN.

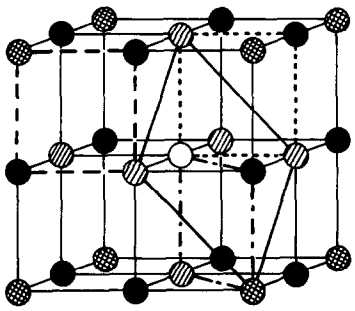

FIG. 1. Cubic unit cell for the $TiN_{0.75}$ model structure. ●, N atoms; ○, vacancy; ◍, $Ti^{[4]}$ atoms; ●, $Ti^{[6]}$ atoms; ---, (100) plane, cut 1; ···, (100) plane, cut 2; -·-·-, (110) plane; —, (111) plane.

Contrary to (*1, 2*) a Hedin–Lundqvist exchange potential (*15*) was employed for the present band structure calculations. Further computational details can be found in Refs. (*1, 2*).

Table I shows the input data for the APW band structure calculation.

Results

(*a*) *Band Structure and DOS*

Figure 2 shows the band structures of TiN and for ordered $TiN_{0.75}$. In order to facilitate the comparison the band structure of TiN is drawn for a simple cubic instead of the face-centered cubic Brillouin zone. So-called "vacancy band states" with a relatively large amount of charge in the vacancy sphere are encircled. As opposed to $TiC_{0.75}$ they all lie below the Fermi level

TABLE I

INPUT PARAMETERS FOR THE APW BAND STRUCTURE CALCULATIONS OF ORDERED $TiN_{0.75}$ AND OF TiN (IN au)

Quantity	Region	Value for $TiN_{0.75}$	Value for TiN
Lattice constant		8.00315	8.01576
Atomic sphere radius	$Ti^{[4]}$, $Ti^{[6]}$	2.02996	2.12903
	N, $\square_N$	1.97161	1.87885

Note. The lattice parameter for $TiN_{0.75}$ has been taken from Ref. (*16*).

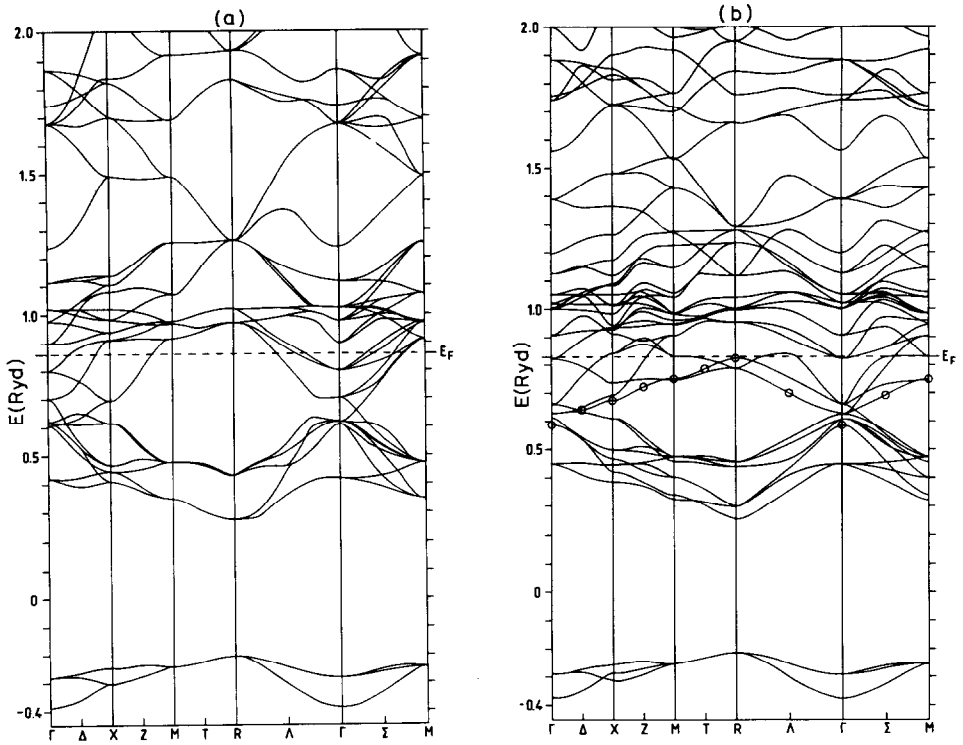

FIG. 2. Band structure of TiN (a) and ordered $TiN_{0.75}$ (b) with respect to the constant muffin-tin potential between the spheres. The band structure of TiN has been backfolded into the small Brillouin zone corresponding to the cubic unit cell shown in Fig. 1. So-called "vacancy states" are encircled in b.

E_F. In Table II a charge analysis (*17*) of the vacancy states is shown. Compared with the substoichiometric titanium carbide, the local charge in the empty nitrogen sphere has substantially increased whereas the partial 3*d* charges in both the $Ti^{[4]}$ and $Ti^{[6]}$ spheres have decreased. This fact will be discussed further in Subsection c of this section, where the charge densities for some vacancy states will be shown. The authors are prepared to provide, on request, a list of all calculated eigenvalues and their partial local *l*-like charges.

Figure 3 displays the DOS of TiN and ordered $TiN_{0.75}$. The first and second DOS peaks, mainly formed by nitrogen 2*s* ("*s* band") and N 2*p* states ("p band"), respectively, show reduced width and intensity in the substoichiometric nitride. The DOS in the energy region between −0.20 and 0.42 Ryd with respect to E_F has mainly Ti 3*d* character ("Ti 3*d* band"). In the case of $TiN_{0.75}$ the DOS in the *d* band is distinctly increased below E_F. In the lower part of the *d* band, two additional peaks appear with an appreciable amount of local partial *s* and *p* DOS, respectively, in the vacancy sphere. These two peaks, which can therefore be attributed to "vacancy" states, have also been found in the KKR-CPA DOS for substoichiometric titanium nitrides. Figure 4 compares the total DOS of the present calculation with the one obtained by the KKR-CPA method (*9, 10*). The two DOS curves are in good agreement, except that the very sharp second peak of our calculation is broad in the CPA calculation. The very large DOS at the

TABLE II

CHARGE ANALYSIS OF STATES BELONGING TO THE VACANCY BAND OF ORDERED $TiN_{0.75}$ AND ENCIRCLED IN FIG. 2b

Irr. rep.	E (Ryd)	N sphere (full) total	$Ti^{[4]}$ sphere								N sphere (empty)		$Ti^{[6]}$ sphere total	q_{out}
			s	p	d	d_{z^2}	$d_{x^2-y^2}$	d_{xy}	(d_{xz}, d_{yz})	Total	s	Total		
Γ_1	0.589	2.26	6.03	—	29.34	29.34	—	—	—	35.38	27.32	27.34	0.01	35.00
Δ_1	0.642	10.11	3.61	0.57	32.08	30.46	1.62	—	—	36.37	23.09	23.65	0.87	29.01
X_1	0.676	5.61	2.64	1.57	37.49	35.32	2.17	—	—	41.77	24.45	24.81	0.02	27.79
Z_1	0.723	5.40	2.26	2.83	33.70	32.43	1.23	—	0.04	38.88	24.67	25.58	0.36	29.78
M_1	0.750	3.89	1.27	4.84	34.57	34.57	—	—	—	40.74	24.85	25.38	0.11	29.87
T_1	0.786	2.41	0.21	8.50	27.08	1.29	—	—	25.78	35.80	14.84	16.27	0.64	44.88
R_1	0.827	2.43	—	15.09	—	—	—	—	—	15.09	29.15	29.19	0.13	53.15
Δ_1	0.699	4.98	2.66	1.74	35.12	32.85	—	0.55	1.72	39.62	20.60	22.61	2.64	30.15
Σ_1	0.692	8.30	3.14	1.50	30.72	29.52	1.12	0.09	—	35.44	24.00	25.07	0.52	30.66
S_1	0.747	4.39	1.92	3.86	32.96	31.92	0.49	—	0.56	38.80	23.25	24.91	0.83	31.05

Note. The energies (in Rydbergs) are given with respect to the constant muffin-tin potential between the spheres. All charges are given in percentages. The data for $Ti^{[4]}$ and N correspond to three muffin-tin spheres.

Fermi level is not confirmed by experiment and it seems to be an artifact of our highly symmetric long-range ordered model structure.

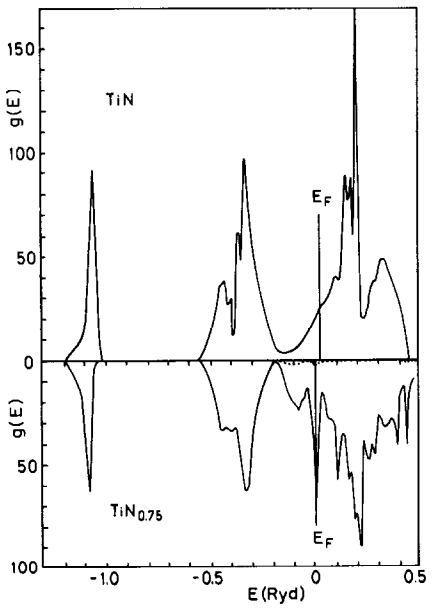

FIG. 3. Total DOS (—) and vacancy DOS (···) for TiN and ordered $TiN_{0.75}$ in units of states per Rydberg, per spin, and per cubic unit cell. (The cubic unit cell contains four formula units.) The curves are adjusted to coincide in the bottom of the N 2*s* band. The Fermi level of $TiN_{0.75}$ is chosen as energy zero.

Table III displays the band widths and the relative positions of the Fermi levels for TiN and $TiN_{0.75}$. As in the carbide the introduction of vacancies reduces the band widths of the *s* and *p* bands without changing the *s*–*p* band gap. The width of the occupied *d* band (where the vacancy peaks are also found) slightly increases in the substoichiometric nitride. The Fermi level decreases in the nitride compared to the bottoms of the *s* and the *p* bands due to an increase of the DOS in the occupied region of the *d* band.

Figure 5 shows the partial local nitrogen *s*

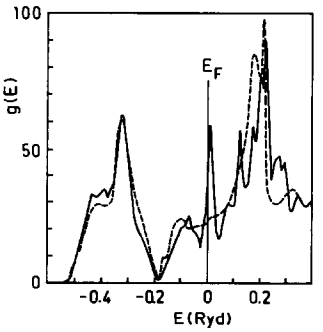

FIG. 4. The total DOS for ordered $TiN_{0.75}$ (—) compared with the total DOS from the KKR-CPA calculation (----) (*9*, *10*). The same units as for Fig. 3 are used.

TABLE III

BAND WIDTHS AND BAND GAPS (IN RYDBERGS) FOR ORDERED $TiN_{0.75}$ AND FOR TiN

	Band	$TiN_{0.75}$	TiN
Band width	s	0.156	0.180
	p	0.376	0.403
	Occupied d (+ vacancy)	0.201	0.190
Band gap	s–p	0.472	0.464
E_F (with respect to bottom of s band)		1.205	1.237
E_F (with respect to bottom of p band)		0.577	0.593

and p, and $Ti^{[4]}$ and $Ti^{[6]}$ $3d$ DOS of $TiN_{0.75}$. As in the carbide the main contribution to the vacancy peaks comes from the $Ti^{[4]}$ $3d$ states. In the p band the partial local Ti $3d$ DOS is smaller than in the carbide, indicating reduced p–d bonding.

Figure 6 displays the local partial DOS in the vacancy sphere from the present calculation and from the CPA-KKR calculation. For both calculations the first peak is almost exclusively formed by vacancy s states and the second peak by vacancy p states. As in the total DOS the second peak in the CPA-DOS is much more diffuse, indicating a considerably reduced lifetime of the vacancy p states. The greater intensities of the CPA peaks are caused by the fact that in the CPA method the DOS curve for the vacancy does not refer to the corresponding atomic sphere, but to a cube circumscribed to it.

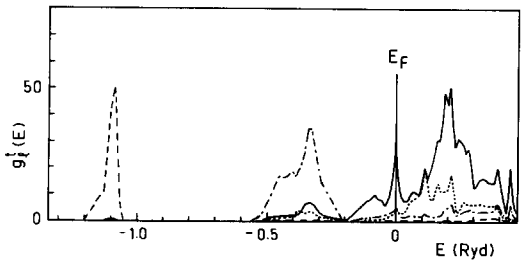

FIG. 5. Main partial local DOS components for $TiN_{0.75}$. The same units and conventions as for Fig. 3 are used. ---, N $2s$ DOS; -·-·-, N $2p$ DOS; ···, $Ti^{[6]}$ $3d$ DOS; —, $Ti^{[4]}$ $3d$ DOS.

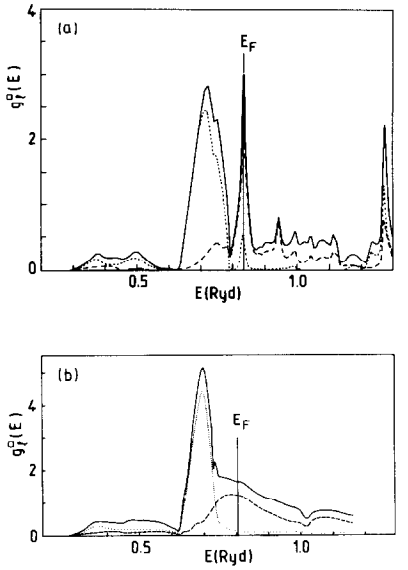

FIG. 6. DOS in the vacancy sphere of ordered $TiN_{0.75}$ (a) and according to the KKR-CPA calculation (b). The same units as for Fig. 3 are used. —, total DOS; ···, s DOS; (---), p DOS.

The crystal field of D_{4h} symmetry splits the $Ti^{[4]}$ $3d$ DOS into d_{z^2}, $d_{x^2-y^2}$, d_{xy} and (d_{xz}, d_{yz}) components. (For description of the orbitals of the $Ti^{[4]}$ atom, a local coordinate system is used, in which the z axis points from the Ti atom to the vacancy and the x and y axes point to the neighboring C atoms.) The first two components are displayed in the upper and the second two in the lower part of Fig. 7.

Only the $d_{x^2-y^2}$ components of the $Ti^{[4]}$ atoms can form $s(p) - d\sigma$ bonds with N $2s$ and $2p$ states and therefore occur in the s and p band. The d_{z^2} component of the $Ti^{[4]}$ atoms, which corresponds to orbitals pointing toward the vacancy, forms rather long d–d σ bonds across the vacancy sites. Therefore the d_{z^2} component dominates at the bottom of the d band and in the vacancy peaks. Similarly, the (d_{xz}, d_{yz}) states, having a reduced possibility of forming p–d π bonds, are now more involved in $Ti^{[4]}$–$Ti^{[4]}$ d–d σ bonding and contribute largely to the DOS of the d band, but only little to the DOS of the p band.

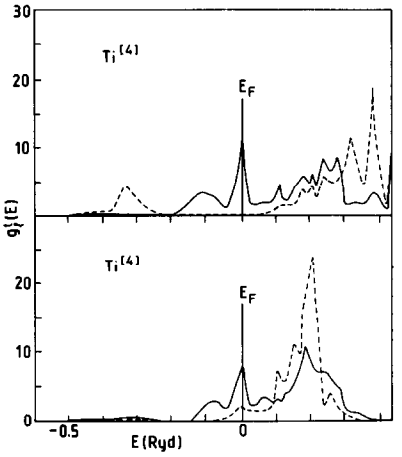

FIG. 7. Split of the partial Ti[4] 3*d* DOS in ordered $TiN_{0.75}$. Top: Ti[4] d_{z^2} (—) and Ti[4] $d_{x^2-y^2}$ (---) DOS. Bottom: Ti[4] (d_{xz}, d_{yz}) (—) and Ti[4] d_{xy} (---) DOS. The same units and the same energy zero as for Fig. 3 are used.

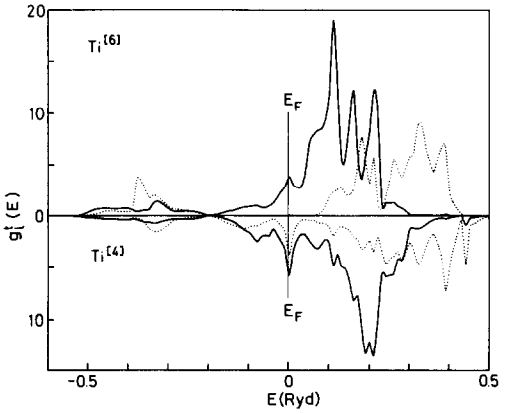

FIG. 8. Comparison of the Ti[6] t_{2g} (—) and e_g (···) DOS with the sums of Ti[4] (d_{xy}, d_{xz}, d_{yz}) (---) and Ti[4] (d_{z^2}, $d_{x^2-y^2}$) (···) DOS. The partial Ti[4] DOS are divided by three to refer to only one muffin-tin sphere. The same units and the same energy zero as for Fig. 3 are used.

The Ti[6] atoms, on the other hand, are in an octahedral crystal field like the Ti atoms in stoichiometric TiN. Figure 8 compares the t_{2g} and e_g components of the Ti[6] 3*d* DOS with the respective sums of the Ti[4] (d_{xy}, d_{xz}, d_{yz}) and the Ti[4] (d_{z^2}, $d_{x^2-y^2}$) components. The partial DOS corresponding to the latter sums are divided by three in order to refer to only one Ti[4] atom. As in $TiC_{0.75}$, the most spectacular effect is the presence of a significant Ti[4] d_{z^2} contribution at the bottom of the *d* band and in the region of the vacancy peak where the Ti[6] partial e_g DOS is very small.

(*b*) *Charge Distribution and Charge Transfer*

The self-consistent APW partial local charges in the muffin-tin spheres and in the interstitial region of TiN and $TiN_{0.75}$ are displayed in Table IV. The charge transfer, defined as the difference between these charges and the charge resulting from a superposition of atomic charge densities, is also given.

In both TiN and $TiN_{0.75}$ charge is transferred from the Ti to the N sphere. The charge transfer in titanium nitride is comparable to that in titanium carbide and increases slightly in both cases with the introduction of vacancies. On the other hand, during the self-consistency procedure the vacancy sphere loses charge in the carbide while the opposite is true for the nitride. Although the effects are small they illustrate nevertheless the increasing importance of Ti–Ti bonding via the vacancy in the nitride.

Table V presents the local partial *s*, *p*, and *d* charges for the different occupied valence bands of TiN and $TiN_{0.75}$ in electrons per muffin-tin sphere (or interstitial volume, respectively).

The overall valence charge in the N sphere increases whereas the interstitial charge as well as the Ti[4] and the Ti[6] 3*d* charges decrease.

In the *s* band slightly more charge is found in the N sphere and less in the interstitial region, indicating the greater localization of the N 2*s* states.

In the *p* band the Ti[4] 3*d* charge and to a lesser extent also the Ti[6] 3*d* charge as well

TABLE IV

SELF-CONSISTENT APW AND SUPERPOSED ATOMIC CHARGES FOR TiN AND FOR ORDERED $TiN_{0.75}$ IN ELECTRONS PER ATOMIC SPHERE

		Ti sphere	N sphere	Interstitial
TiN	APW self-consistent	19.85	6.88	2.27
	Atomic superposed	20.18	6.50	2.32
	Difference	−0.33	0.38	−0.05

		$Ti^{[4]}$ sphere	$Ti^{[6]}$ sphere	N sphere	$\square_N$ sphere	Interstitial
$TiN_{0.75}$	APW self-consistent	19.48	19.51	7.20	0.77	2.17
	Atomic superposed	19.83	19.91	6.74	0.70	2.17
	Difference	−0.35	−0.40	0.46	0.07	0.00

Note. The interstitial charge for TiN corresponds to the region outside the muffin-tin spheres in the rhombohedral unit cell and for $TiN_{0.75}$ to one-fourth of the interstitial volume in the cubic unit cell.

as the interstitial charge are greatly reduced, thus indicating fewer p–d bonds. Also the $2p$ states become more localized in the nonstoichiometric compound as can be deduced from the slightly larger $2p$ charge in the N sphere. Some charge found in the vacancy sphere is due to the overlap of p and vacancy bands.

TABLE V

APW PARTIAL CHARGES FOR ORDERED $TiN_{0.75}$ AND FOR TiN IN ELECTRONS PER ATOMIC SPHERE

		$TiN_{0.75}$					TiN		
Band		$Ti^{[6]}$	$Ti^{[4]}$	N	$\square_N$	Interstitial	Ti	N	Interstitial
s	s	0.03	0.02	1.57	—		0.03	1.51	
	p	0.06	0.04	—	—		0.07	—	
	d	0.05	0.03	—	—		0.06	—	
	Total	0.15	0.10	1.57	—	0.21	0.17	1.51	0.32
p	s	0.07	0.07	0.02	0.05		0.09	0.02	
	p	0.16	0.12	3.26	0.02		0.18	3.10	
	d	0.97	0.51	0.02	0.01		1.05	0.02	
	Total	1.21	0.71	3.31	0.09	1.16	1.35	3.14	1.51
d (+ vacancy)	s	—	0.02	0.00	0.47		—	—	
	p	—	0.04	0.23	0.14		0.01	0.15	
	d	0.41	0.94	0.04	0.02		0.59	0.02	
	Total	0.43	0.99	0.28	0.63	0.54	0.61	0.18	0.22
Occupied valence	s	0.10	0.10	1.60	0.52		0.12	1.53	
	p	0.22	0.20	3.49	0.16		0.26	3.25	
	d	1.43	1.48	0.06	0.03		1.70	0.04	
	Total	1.79	1.80	5.16	0.72	1.91	2.13	4.83	2.05

Note. For the interstitial charge the same convention as in Table IV is used.

Comparing the nonstoichiometric titanium nitride with the corresponding carbide, one notices a considerable increase in the vacancy band of both $Ti^{[4]}$ $3d$ charge and of the charge in the vacancy sphere. This means that the d–d bonding of $Ti^{[4]}$ $3d$ states via the vacancy becomes more important.

Further information about bonding mechanisms can be gained from the split of the Ti $3d$ charge into its components which is presented in Table VI.

The decrease of the $Ti^{[6]}$ $3d$ charge in the p and d bands is shown to be a decrease of t_{2g} charge. The $Ti^{[6]}$ t_{2g} orbitals are less involved in d–d bonding with their nearest Ti ($Ti^{[4]}$) neighbors.

For the $Ti^{[4]}$ $3d$ charge, the d_{z^2} and (d_{xz}, d_{yz}) components are clearly reduced in the p band but are the largest contributors to the DOS in the vacancy bands. Both effects together lead to the same valence d charge in the $Ti^{[4]}$ and $Ti^{[6]}$ spheres of $TiN_{0.75}$. The Ti t_{2g} charge contribution is considerably larger in stoichiometric TiN.

From the fact that the $Ti^{[4]}$ d_{xy} and the $Ti^{[6]}$ t_{2g} charge component decrease (Table VI) it can therefore be concluded that reduced d–d σ bonding between $Ti^{[4]}$ and $Ti^{[6]}$ atoms occurs in the substoichiometric nitride. Furthermore, $Ti^{[4]}$ d_{z^2} and (d_{xz}, d_{yz}) states are involved in d–d bonds as in the case of $TiC_{0.75}$. However, in the nitride these bonds lead to a greater amount of charge in the vacancy sphere.

(c) *Electron Densities*

The valence electron densities were calculated from the APW wave functions as described in (*2*).

Figure 9 presents the valence electron densities of $TiN_{0.75}$ in two inequivalent cuts of the (100) plane together with the corresponding plot for TiN. In Fig. 10 the corresponding plots in the (110) plane are shown.

In contrast to the carbide the valence electron density barely changes with the introduction of vacancies in the $Ti^{[4]}$–N direction. In the substoichiometric nitride the valence electron density in the $Ti^{[6]}$ sphere is only slightly lower if the $Ti^{[6]}$–N direction is considered. In the $Ti^{[4]}$–$Ti^{[6]}$ direction, the $Ti^{[4]}$ electron density is reduced in $TiN_{0.75}$ and enhanced in $TiC_{0.75}$ compared with the stoichiometric compounds. Therefore, it seems that the covalent $Ti^{[4]}$–$Ti^{[6]}$ d–d σ bonds are weakened in the nitride and strengthened in the carbide.

Evidence for a different bonding situation in the substoichiometric carbide and nitride can also be seen in Fig. 11, where the difference between the valence electron densities of $TiN_{0.75}$ and TiN is plotted in the (111) plane (omitting the $2s$ contribution).

TABLE VI

SPLIT OF THE PARTIAL Ti $3d$ CHARGE IN ORDERED $TiN_{0.75}$ AND IN TiN

	$TiN_{0.75}$						TiN	
	$Ti^{[4]}$				$Ti^{[6]}$		Ti	
Band	d_{z^2}	$d_{x^2-y^2}$	d_{xy}	(d_{xz}, d_{yz})	e_g	t_{2g}	e_g	t_{2g}
p	0.04	0.24	0.10	0.13	0.55	0.38	0.58	0.46
d (+ vacancy)	0.33	0.01	0.09	0.51	0.01	0.41	0.01	0.58
Occupied valence	0.38	0.27	0.19	0.64	0.61	0.79	0.65	1.05

Note. All charges are given in number of electrons per atomic sphere.

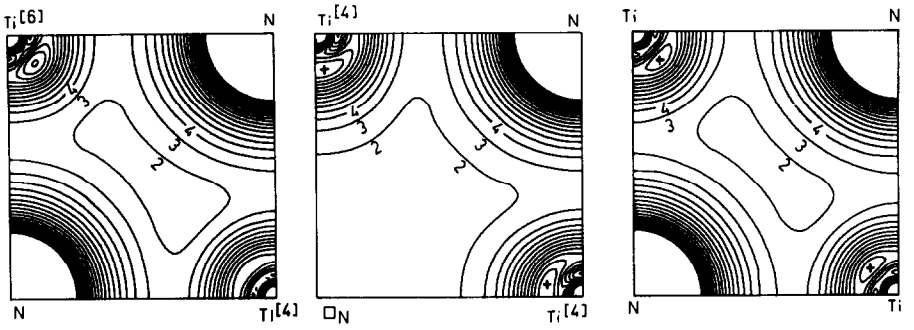

FIG. 9. Valence electron densities in the (100) plane of $Ti_3^{[4]}Ti^{[6]}N_3\square_N$ and TiN in unit of 10^{-1} $e/Å^3$. Left: $TiN_{0.75}$, cut 1; center: $TiN_{0.75}$, cut 2; right: TiN. Local maxima are marked with "+".

In substoichiometric $TiN_{0.75}$ there is a positive electron density difference in the region between the $Ti^{[4]}$ atoms, but a mainly negative density difference between the $Ti^{[4]}$ and $Ti^{[6]}$ atoms. Compared to $TiC_{0.75}$, where the density difference between the $Ti^{[4]}$ and $Ti^{[6]}$ atoms is positive, this means weaker $Ti^{[4]}$–$Ti^{[6]}$ d–d σ bonds in $TiN_{0.75}$ than in TiN. Consequently, the $Ti^{[6]}$ lattice sites seem to be less stabilized in the nitride than in the carbide.

Analogous to $TiC_{0.75}$ two new bond types occur in substoichiometric titanium nitride apart from the usual p–d σ, p–d π, and d–d σ bonds (*18*).

The first new bond type is illustrated in Fig. 12 where the electron densities in the (100) plane are shown for the "vacancy band" states Γ_1, Δ_1, and X_1. As in $TiC_{0.75}$ (*2*) the valence electron densities are increased in the direction from the $Ti^{[4]}$ atoms toward the vacancy, creating weak bonding states of s symmetry in the vacancy sphere (bonding d_{z^2}–$\square_N$–d_{z^2} σ interactions). Energetically these states can be found in the first vacancy peak of the DOS. The corresponding antibonding states (of p symmetry in the vacancy sphere) are found in the second vacancy peak of the DOS. Bonding interactions via the vacancy can also occur between two $Ti^{[4]}$ d_{z^2} orbitals oriented at right angles to each other.

Whereas in $TiC_{0.75}$ only the bonding d_{z^2}–$\square_N$–d_{z^2} states in the first vacancy peak are occupied, some of their antibonding counterparts are already situated below E_F

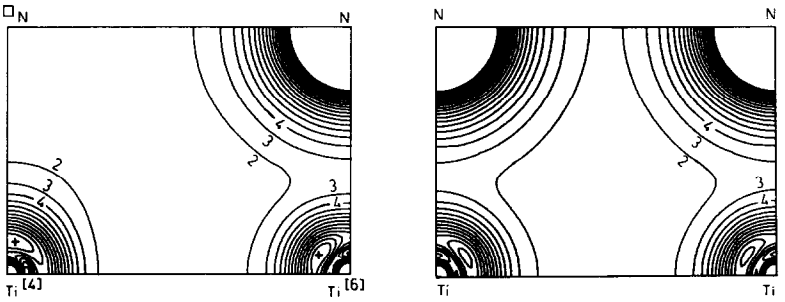

FIG. 10. Valence electron densities in the (110) plane of $Ti_3^{[4]}Ti^{[6]}N_3\square_N$ and TiN in units of 10^{-1} $e/Å^3$. Left: $TiN_{0.75}$; right: TiN. Local maxima are marked with "+".

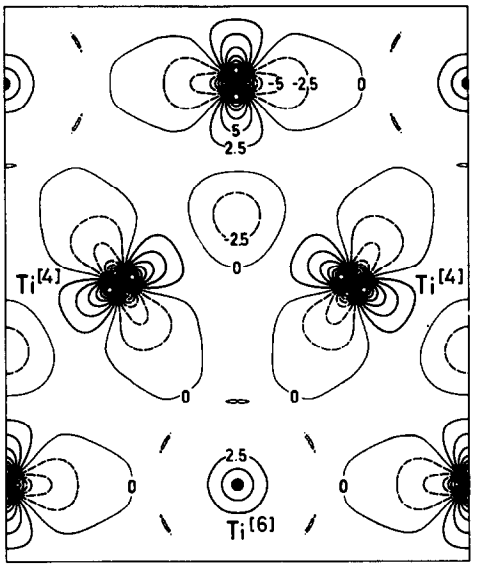

FIG. 11. Difference between the valence electron densities of $TiN_{0.75}$ and TiN (omitting the electron density of the 2*s* band) in the (111) plane in units of 10^{-2} $e/Å^3$.

in $TiN_{0.75}$, partly compensating their stabilizing effect.

The second new bond type occurs between the d_{xz} and d_{yz} orbitals of the $Ti^{[4]}$ atoms around the vacancy. They can form better overlapping (stronger) d–d σ bonds than the t_{2g} orbitals of stoichiometric TiN because they are less involved in p–d π bonding with nitrogen p orbitals. These "octahedral bonds" are illustrated by the electron density plot for a state of X_3 symmetry in the (111) plane (Fig. 13). Moreover, in the substoichiometric nitride a larger number of bonding states forming octahedral bonds are situated below the Fermi level than in the corresponding carbide. Therefore, the stabilization of the $Ti^{[4]}$ octahedra is more effective for the substoichiometric nitride than for the substoichiometric carbide.

(*d*) *Spectral Properties*

In recently measured photoelectron (*11, 12, 19*), K (*20*), and L (*21*) X-ray emission spectra for substoichiometric titanium nitrides, a vacancy peak appears at approximately 2 eV below the Fermi level whose intensity grows with increasing vacancy concentration. Energy loss spectra (*22*) also show the existence of these vacancy states whereas optical measurements (*23*) could be interpreted without assuming vacancy states below the Fermi level.

Although the assumption of long-range ordered vacancies is not valid for real TiN_x samples, it should be possible to explain the main features of the experimental spectra using the results of our band structure calculation.

Figure 14 shows the experimental XPS spectra of Porte *et al.* (*12*) of $TiN_{0.94}$ and $TiN_{0.75}$ together with the calculated broadened DOS for TiN and $TiN_{0.75}$. As indicated by Porte *et al.*, a spectrometer

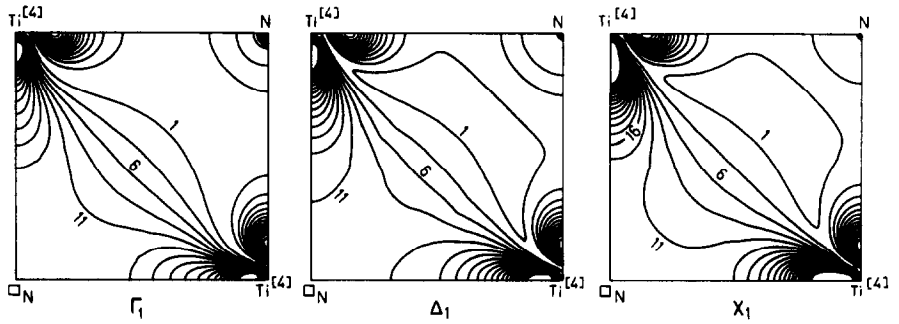

FIG. 12. Electron densities for the "vacancy band" states Γ_1, Δ_1, and X_1 of $TiN_{0.75}$ in the (100) plane (cut 2) in units of 10^{-2} $e/Å^3$.

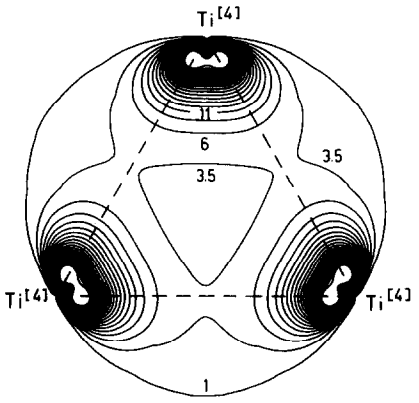

FIG. 13. Electron density for the state X_3 of $TiN_{0.75}$ in the (111) plane in units of 10^{-2} $e/Å^3$.

function of half-width 1.1 eV was used for broadening the theoretical DOS. In the present work the influence of site-, *l*-, and energy-dependent photoabsorption cross sections and of life-time broadening is neglected. Qualitatively the calculated curves agree well with the measured spectra. The main peak is independent of the vacancy contents both in theory and in experiment. The smaller peak becomes larger with an increasing number of vacancies and a shoulder at a binding energy of roughly 2 eV develops which can be ascribed to the vacancy states. The measured XPS spectra of Höchst *et al.* (*11*) are in substantial agreement with the results of Porte *et al.* (*12*). Minor differences between the two measurements such as the split of the low binding energy peak into a double peak (*11*) for an increasing number of vacancies can be attributed to the better resolution in (*11*).

A quantitative comparison of the measured spectra with our broadened DOS shows that the calculated peaks are too narrow and shifted to lower binding energies. Moreover, the peak at lower binding energy is overestimated even for stoichiometric titanium nitride. Similar deviations were found between the spectra of TiN_x calculated by means of the KKR-CPA method (*24*) and experimental spectra. The shift and narrowing of the theoretical peaks was interpreted in (*24*) as defects of the density functional method in the local density approximation, which was also used for the present band structure calculation. The too high intensity at lower binding energies, even for stoichiometric TiN, can most probably be explained by the assumption of long-range order for the vacancies, leading to rather sharp vacancy peaks, and by the neglect of life-time broadening and photoabsorption cross-section effects.

In (*24*) it has been shown that the photoabsorption cross section of the Ti 4*p* electrons is much larger than that of the Ti 3*d* electrons, while the N 2*p* cross section is almost negligible. Therefore, the XPS is dominated by the contribution of the Ti 4*p* electrons, although their partial local DOS is very small. According to our calculations for stoichiometric TiN, the Ti 4*p* DOS is similar in shape to the total DOS of the *p* band (above 3 eV), but is practically zero below a binding energy of 3 eV. A proper

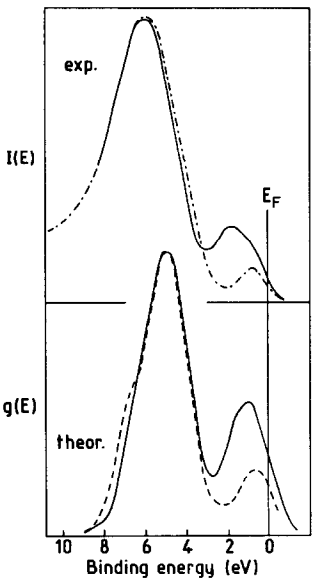

FIG. 14. Comparison of the experimental XPS spectra of Porte *et al.* (*12*) of $TiN_{0.94}$ (–·–·–) and $TiN_{0.75}$ (—) with the calculated broadened DOS for TiN (– – –) and $TiN_{0.75}$ (—).

calculation of the photoabsorption cross sections would certainly improve the intensity ratio of the two peaks in the XPS of TiN (notice that the intensities of the spectra are given in arbitrary units).

Figure 5 shows clearly that the vacancy states are not exclusively formed by Ti 3*d* states. This is in agreement with constant initial state (CIS) measurements on TiN_x (*19*) which lead to the conclusion that approximately 25% of the intensity of the vacancy peak can be attributed to non-*d*-like states.

Figure 15 displays Ti–K XES measurements for substoichiometric titanium nitride (*20*) together with the corresponding spectra calculated by means of the KKR-CPA method (*20*) and the spectra based on the present APW band structure calculation. The latter spectra were determined by broadening the partial Ti 4*p* DOS of TiN and $TiN_{0.75}$ without considering the energy dependence of the transition moments that are usually small (*25*). The Ti 4*p* DOS was broadened by a Lorentzian with a parameter Γ_0 of 0.5 eV for the core states and a parameter W of 1 eV for the energy-dependent valence-state life-time broadening. Apart from that, spectrometer broadening with a half-width S of 1 eV was also taken into account (*25*).

Both theoretical approaches give a good description of the trends. In contrast to the XPS, both the main peak and the vacancy peak are shifted to lower binding energies with increasing vacancy concentration. As in the case of XPS the theoretical peaks are too narrow and at too low binding energies, and the vacancy peak is overestimated. The former two effects may again be caused by the density functional theory in the local density approximation.

Conclusions

For $TiN_{0.75}$ only short-range order of vacancies has been found experimentally. At first sight, the KKR-CPA method seems to be most appropriate for the description of such a compound, where this kind of order can be treated as a perturbation. For substoichiometric titanium nitrides, calculations assuming a random distribution of the vacancies have been performed, and DOS (*9, 10*), XPS (*24*) and angle-resolved photoemission spectra (*26*) have been obtained. For investigations of the bonding

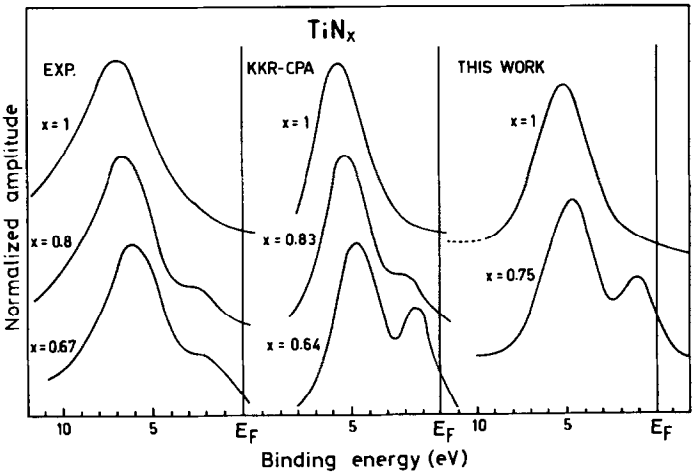

FIG. 15. Left: Ti K-XES measurements (*20*); center: spectra calculated by means of the KKR-CPA method (*20*); right: broadened partial Ti 4*p* DOS of TiN and $TiN_{0.75}$ (this work).

situation, however, band structure calculations on ordered model structures seem to be more useful, especially if the influence of vacancies on particular bonds of the crystal has to be examined. Such investigations should retain their validity even if the assumed arrangement of atoms is not repeated under translation, but occurs only as a local cluster. In the case of $TiN_{0.75}$ mainly the $Ti^{[4]}$ 3*d* (and 4*p*) electrons are influenced by the presence of vacancies at the nonmetal lattice sites. The $Ti^{[4]}$ d_{z^2} electrons no longer form any strong p–d σ bonds with the N 2*p* electrons. Therefore the contribution to the *p* band of the $Ti^{[4]}$ d_{z^2} electrons is greatly reduced compared with stoichiometric TiN. Instead, the $Ti^{[4]}$ d_{z^2} electrons enter into weak second-neighbor d_{z^2}–$\square_N$–d_{z^2} σ bonds across the vacancy. In $TiN_{0.75}$, bonding and antibonding states corresponding to this interaction bring about two vacancy peaks in the DOS, one of *s* and the other of *p* symmetry in the vacancy sphere. Similar effects can be expected for the Ti $4p_z$ electrons. Although their contribution to the total DOS is small, they determine the shape of the K-XES and, due to their large photoabsorption cross section, also of the XPS (*24*).

In the substoichiometric nitride the $Ti^{[4]}$ d_{xz} and d_{yz} electrons become less involved in p–d bonding with the N 2*p* electrons. Instead, they form octahedral d–d bonds with each other, which are stronger than in TiN, and thus stabilize the $Ti^{[4]}$ octahedra around the vacancy. These octahedral bonding states are even more important for the substoichiometric nitride than for the corresponding carbide (*2*) because more states of that kind are occupied in the nitride. Apart from that, the individual octahedral bonding states form stronger bonds in the nitride compared with the carbide. Nevertheless, the additional metal–metal bonds cannot compensate for the loss in stability because of the more pronounced decrease of p–d bonds by the introduction of vacancies, which leads to a decrease in the cohesive energy (*20*).

An interesting result of our present calculation is the influence of the vacancies on the $Ti^{[4]}$–$Ti^{[6]}$ d–d σ bonds. These bonds are strengthened by carbon vacancies in $TiC_{0.75}$, but are weakened by the nitrogen vacancies in $TiN_{0.75}$, thus allowing metal vacancies to be formed on the $Ti^{[6]}$ sublattice for TiN_x, but not for TiC_x. Under special experimental conditions such metal vacancies occur in TiN_x samples of high N contents, but not in TiC_x samples (*7*).

The DOS derived from APW and from CPA calculations are in good agreement. As expected, the KKR-CPA curves are broader, an effect which is particularly pronounced for the second vacancy peak whose shape seems to be an artifact of the highly symmetric long-range-ordered defect structure used for the APW calculation.

Acknowledgment

We gratefully acknowledge financial support by the Hochschuljubiläumsstiftung der Stadt Wien.

References

1. J. Redinger, R. Eibler, P. Herzig, A. Neckel, R. Podloucky, and E. Wimmer, *J. Phys. Chem. Solids* **46,** 383 (1985).
2. J. Redinger, R. Eibler, P. Herzig, A. Neckel, R. Podloucky, and E. Wimmer, *J. Phys. Chem. Solids* **47,** 387 (1986).
3. H. Nowotny, *Radex Rundschau* **2,** 41 (1953).
4. F. Schlapansky, P. Herzig, R. Eibler, and A. Neckel, to be published.
5. S. Nagakura, T. Kusunoki, F. Kakimoto, and Y. Hirotsu, *J. Appl. Crystallogr.* **8,** 65 (1975); S. Nagakura and T. Kusunoki, *J. Appl. Crystallogr.* **10,** 52 (1977).
6. M. D. Banus, T. B. Reed, and A. J. Strauss, *Phys. Rev. B* **5,** 2775 (1972).
7. L. E. Toth, "Transition Metal Carbides and Nitrides," Academic Press, London (1971).
8. J. Billingham, P. S. Bell, and M. H. Lewis, *Acta Crystallogr. A* **28,** 602 (1972); M. Sauvage and E. Parthe, *Acta Crystallogr. A* **28,** 607 (1972).

9. P. MARKSTEINER, P. WEINBERGER, A. NECKEL, R. ZELLER, AND P. H. DEDERICHS, *Phys. Rev. B* **33,** 812 (1986).
10. J. KLIMA, G. SCHADLER, P. WEINBERGER, AND A. NECKEL, *J. Phys. F* **15,** 1307 (1985).
11. H. HÖCHST, R. D. BRINGANS, P. STEINER, AND T. WOLF, *Phys. Rev. B* **25,** 7183 (1982).
12. L. PORTE, L. ROUX, AND J. HANUS, *Phys. Rev. B* **28,** 3214 (1983).
13. J. KLIMA, *Czech. J. Phys. B* **30,** 905 (1980).
14. L. F. MATTHEISS, J. H. WOOD, AND A. C. SWITENDICK, *in* "Methods in Computational Physics," Vol. 8, p. 63, Academic Press, New York (1968).
15. L. HEDIN AND S. LUNDQVIST, *J. Phys. Paris* **33,** C3–73 (1972).
16. I. A. BRYTOV, B. E. BLEKHER, AND V. S. NESHPOR, *Sov. Phys. Techn. Phys.* **24,** 588 (1979).
17. A. NECKEL, P. RASTL, R. EIBLER, P. WEINBERGER, AND K. SCHWARZ, *J. Phys. C* **9,** 579 (1976).
18. A. NECKEL, K. SCHWARZ, R. EIBLER, P. WEINBERGER, AND P. RASTL, *Ber. Bunsenges. Phys. Chem.* **79,** 1053 (1975).
19. R. D. BRINGANS AND H. HÖCHST, *Phys. Rev. B* **30,** 5416 (1984).
20. E. BEAUPREZ, C. F. HAGUE, J. M. MARIOT, F. TEYSSANDIER, J. REDINGER, P. MARKSTEINER, AND P. WEINBERGER, *Phys. Rev. B* **34,** 886 (1986).
21. YU. N. KUCHERENKO, L. M. SHELUDCHENKO, V. Z. KHRINOVSKY, AND V. V. NEMOSHKALENKO, *J. Phys. Chem. Solids* **45,** 319 (1984).
22. J. PFLÜGER, J. FINK, W. WEBER, AND K. P. BOHNEN, *Phys. Rev. B* **30,** 1155 (1984).
23. K. KÖHLER, H. P. GESERICH, AND A. N. CHRISTENSEN, *Z. Phys. B* **62,** 319 (1986).
24. J. REDINGER, P. MARKSTEINER, AND P. WEINBERGER, *Z. Phys. B* **63,** 321 (1986).
25. K. SCHWARZ AND A. NECKEL, *Ber. Bunsenges. Phys. Chem.* **79,** 1071 (1975).
26. J. REDINGER, P. WEINBERGER, AND A. NECKEL, submitted for publication.